RSC Advances

PAPER

View Article Online
View Journal | View Issue

Cite this: *RSC Adv.*, 2025, **15**, 19204

Targeting apoptotic pathways in cancer: design, synthesis, and molecular docking studies of 1,3,5-trisubstituted-1*H*-pyrazole derivatives with Bcl-2 inhibition and DNA damage potential†

Ahmed Temirak, *[a] Ahmed A. F. Soliman,[b] Mohamed B. Shalaby,[c] Mariam G. Eshak,[d] Wagdy K. B. Khalil,[d] Zahid Shafiq [e] and Nader M. Boshta*[f]

The search for new anticancer agents targeting apoptotic and autophagic pathways is crucial due to their roles in cellular homeostasis and cancer cell elimination. In this study, we synthesized and evaluated a series of 1,3,5-trisubstituted-1*H*-pyrazole derivatives as potential inhibitors of Bcl-2, a key regulator of apoptosis and autophagy. Several compounds activated pro-apoptotic proteins Bax, p53, and Caspase-3. Structure–activity relationship (SAR) studies assessed the cytotoxic effects of the compounds on MCF-7, A549, and PC-3 cancer cell lines. Compounds **4**, **5**, **6b**, **6c**, **7**, **8**, **10b**, **10c**, and **12b** showed significant cytotoxicity against MCF-7 cells (IC_{50}: 3.9–35.5 μM), with similar activity observed against A549 and PC-3 cell lines. Compounds **6c**, **8**, **10b**, and **10c** also induced DNA damage, as evidenced by increased comet tail length, suggesting they cause genotoxic stress through DNA strand breaks. SAR analysis highlighted the importance of chlorophenyl, thiazole, and sulfonamide groups in enhancing cytotoxicity. Molecular docking confirmed high binding affinity of compounds **10b** and **10c** to Bcl-2 through key hydrogen bonding interactions. These findings suggest that the 1,3,5-trisubstituted-1*H*-pyrazole derivatives effectively target Bcl-2, activate apoptotic pathways, and induce DNA damage, making them promising candidates for further anticancer investigation.

Received 23rd March 2025
Accepted 24th May 2025

DOI: 10.1039/d5ra02046h

rsc.li/rsc-advances

Introduction

Cancer is a significant global health burden and ranks as the second-leading cause of death, following cardiovascular diseases.[1,2] It remains one of the most challenging diseases to treat, characterized by uncontrolled cell proliferation and the ability to avoid programmed cell death mechanisms. The toxicity of existing anticancer drugs and the limited effectiveness of current chemotherapies are major obstacles in the fight against cancer. Consequently, the primary goal in the field of organic medical chemistry, particularly in targeted therapeutic strategies, is to design and discover effective and selective antitumor agents.[3] Such strategies involve inducing apoptosis and autophagy.

Apoptosis, a form of programmed cell death, is essential for maintaining cellular homeostasis and eliminating damaged cells. Tumor cells are known to have dysregulated apoptotic machinery, enabling tumor cells to survive longer than they should.[4] Autophagy, a cellular degradation process, plays a dual role in cancer. While autophagy can provide nutrients to support cancer cell survival under stress, it can also promote cell death when overly activated.[5] The balance between these processes is crucial in determining cell fate. One of the key regulators of both apoptosis and autophagy is the B-cell lymphoma 2 (Bcl-2) protein family.

Bcl-2 as a therapeutic target, Bcl-2 is an anti-apoptotic protein that is overexpressed in various cancers, contributing to tumorigenesis and resistance to chemotherapy.[6] Therefore, targeting Bcl-2 to promote apoptosis and autophagy represents a promising strategy for cancer therapy.[7] Bcl-2 proteins inhibit apoptosis by binding to pro-apoptotic proteins such as BCL-2-associated X protein (BAX) and also modulate autophagy by interacting with Beclin 1, a critical autophagy protein.[8] Bcl-2 inhibitors can disrupt the interaction between Bcl-2 and pro-apoptotic proteins, thereby inducing cell death.[9] Moreover, inhibiting the interaction between Bcl-2 and Beclin 1 can

[a]*Chemistry of Natural and Microbial Products Department, Pharmaceutical and Drug Industries Research Institute, National Research Centre, Dokki, Giza, 12622, Egypt. E-mail: amtemirak@hotmail.com*

[b]*Drug Bioassay-Cell Culture Laboratory, Pharmacognosy Department, National Research Center, Giza 12622, Egypt*

[c]*Toxicology Research Department, Research Institute of Medical Entomology (RIME), General Organisation of Teaching Hospitals and Institutes (GOTHI), Ministry of Health and Population (MoHP), Dokki, P. O. Box 12311, Cairo, Egypt*

[d]*Department of Cell Biology, National Research Centre, 12262 El-Bohouth St., Cairo, Egypt*

[e]*Institute of Chemical Sciences, Bahauddin Zakariya University, Multan, Pakistan*

[f]*Chemistry Department, Faculty of Science, Menoufia University, Shebin El-Koam 32511, Egypt. E-mail: nboshta2@gmail.com*

† Electronic supplementary information (ESI) available. See DOI: https://doi.org/10.1039/d5ra02046h

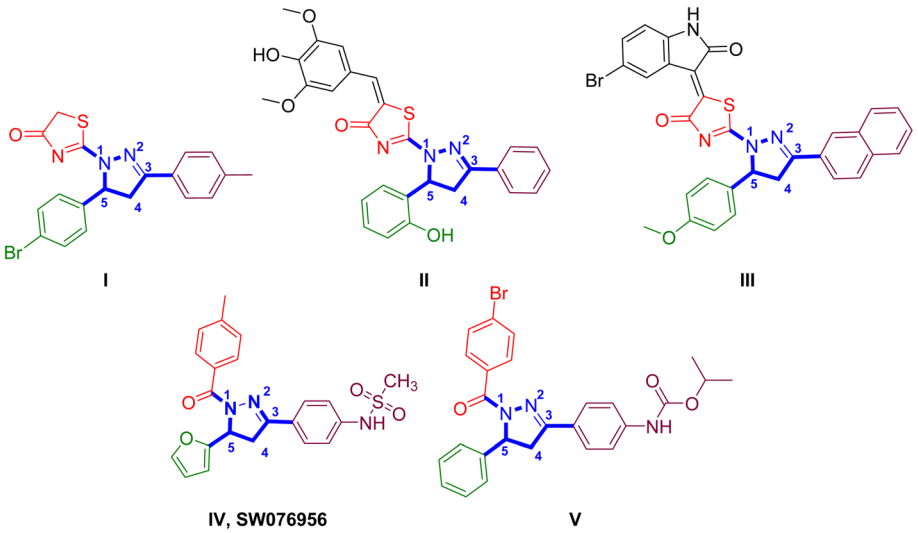

Fig. 1 Examples of reported 1,3,5-trisubstituted-1*H*-pyrazole derivatives with anticancer activities.[11–14]

promote autophagy, which may enhance the anti-tumor effects of Bcl-2 inhibition (Fig. 1).[10,11] By leveraging these insights, our current study aims to further explore the therapeutic potential of Bcl-2 inhibitors.

Recent studies have highlighted the potential of 1,3,5-trisubstituted-1*H*-pyrazole derivatives as promising anticancer agents. These compounds have shown significant antiproliferative activity against various cancer cell lines, making them a focus of medicinal chemistry research. For instance, compound **I** exhibited remarkable antiproliferative effects against MCF-7, B16-F10, and HCT-116 cancer cell lines. Furthermore, this compound demonstrated potent inhibition of key oncogenic proteins, including epidermal growth factor receptor (EGFR) and HER-2, which are critical targets in cancer therapy.[12] Additionally, compound **II**, identified from a separate study, was found to have a selective anticancer influence on colon cancer cell lines, particularly HT-29, where it displayed a log GI_{50} value of −6.37, indicating its efficiency against this cancer type.[13]

Another potent derivative, compound **III**, has shown broad-spectrum anticancer activity with a mean GI_{50} of 0.071 μM and a TGI of 0.76 μM. It exhibited its highest antiproliferative effects on the non-small cell lung cancer line HOP-92, where the GI_{50} was less than 0.01 μM. This compound was also active against other lines, including HCT-116 (GI_{50} = 0.018 μM), CNS cancer line SNB-75 (GI_{50} = 0.0159 μM), ovarian cancer NCI/ADR-RES (GI_{50} = 0.0169 μM), and renal cancer RXF 393 (GI_{50} = 0.0197 μM).[14] In the realm of Bcl-2 inhibition, compound **IV** (**SW076956**) emerged as a potent inhibitor, targeting the Bcl-2 protein involved in apoptosis.[11] Structure–activity relationship studies on this compound led to the development of more selective Bcl-2 inhibitors, such as compound **V**, which specifically disrupts the Bcl-2-Beclin 1 interaction responsible for autophagy regulation while sparing the Bcl-2-Bax interaction critical for apoptosis. This specificity opens new avenues for cancer therapy by promoting autophagic cell death without triggering apoptosis.[11]

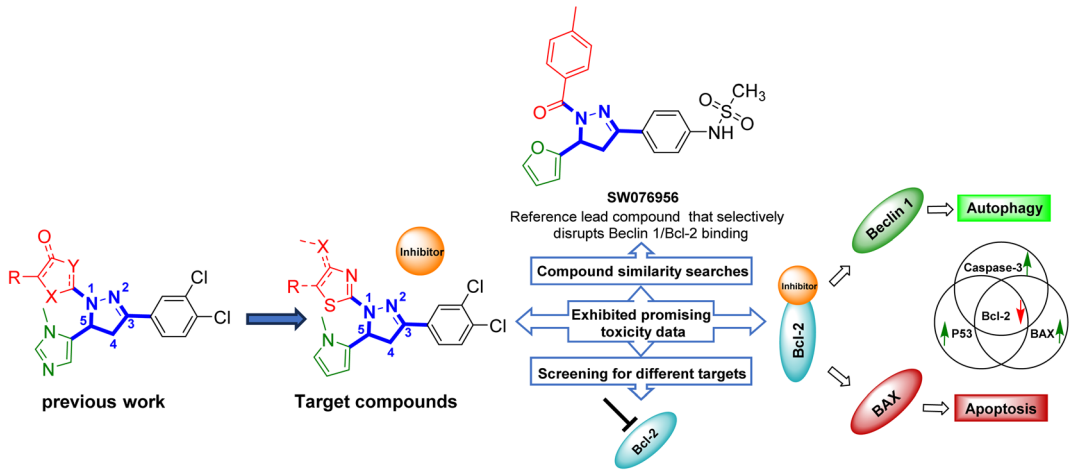

Fig. 2 Design of the new 1,3,5-trisubstituted-1*H*-pyrazole derivatives with proposed Bcl-2 inhibition activities.

In our previous research, we synthesized 1,3,5-trisubstituted-1*H*-pyrazole derivatives and evaluated their anticancer activities, particularly focusing on ERK and RIPK3 kinase inhibition. These compounds were active against ERK and RIPK3 and demonstrated significant cytotoxicity.[15] Building on this success, we synthesized new analogues and investigated their activity, particularly targeting ERK and RIPK3. However, these new compounds were found to be less active in those assays. Despite this reduced activity, they exhibited promising cytotoxicity on several cancer cell lines, that encouraged us to explore their activity on other targets related to apoptosis and autophagy.

Our subsequent screening efforts, including *in vitro* assays for different targets and compound similarity searches in the literature, identified Bcl-2 as a novel target for our pyrazole derivatives. The promising cytotoxicity data of these compounds against cancer cells, combined with their structural similarity to known Bcl-2 inhibitors, specifically compound **SW076956** encouraged us to investigate their ability to inhibit Bcl-2 to develop effective anticancer agents (Fig. 2).[11] The aim of this study is to develop small molecule inhibitors of Bcl-2 with dual functionality in promoting both autophagy and apoptosis. We synthesized different derivatives of our initial compounds to study the structure–activity relationship (SAR) and enhance the potency of Bcl-2 inhibition. Our findings suggest that these novel Bcl-2 inhibitors could serve as potential therapeutic agents for cancer treatment, offering a new strategy to induce cancer cell death through both apoptotic and autophagic pathways (Fig. 2).

Results and discussion

Chemistry

Chalcones are chemical compounds consisting of two aromatic/heterocyclic rings linked by three carbon atoms, forming an α, β-unsaturated carbonyl system. These compounds are abundant in edible plants and are frequently utilized in traditional folk remedies, such as *Angelica*, *Glycyrrhiza*, *Humulus*, and *Scutellaria*. Moreover, chalcones play a crucial role as precursors in the biosynthesis of flavonoids and isoflavonoids. The key characteristic of chalcones lies in their conjugated double bond system and completely delocalized π-electron system present in both aromatic rings. As a result, they exhibit relatively low redox potentials and a high tendency to participate in electron transfer reactions.[16]

The starting material **3** can be prepared using a specific type of aldol-condensation reaction called the base-catalyzed Claisen–Schmidt condensation.[14] This reaction involves the reaction of the commercially available 1-methyl-1*H*-pyrrole-2-carbaldehyde **1** with the commercially available ketone 1-(3,4-dichlorophenyl) ethan-1-one **2**. The reaction takes place in the presence of 10% NaOH as a base, using ethanol as the solvent, and stirring at room temperature for 4 hours. As a result, the final compounds are obtained in the form of yellow powder (Scheme 1). The key

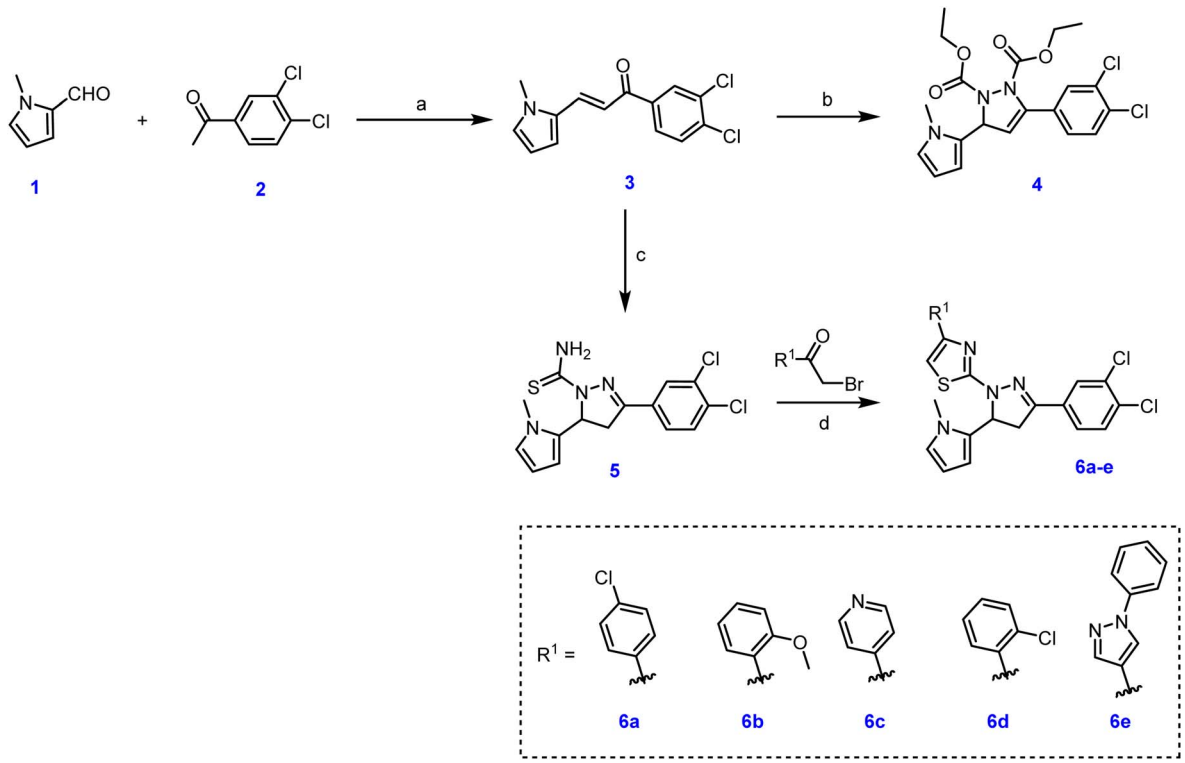

Scheme 1 Synthesis of target compounds **4**, and **6a–e**. Reagents and conditions: (a) NaOH (10% aq.), EtOH, 0 °C–rt, 4 h; (b) diethyl azodicarboxylate, Ph_3P, toluene, rt, 7h, 60%; (c) thiosemicarbazide, NaOH, EtOH, 100 °C, 8 h, 87%; (d) phenacyl bromide derivative, EtOH, 100 °C, 3h, 49–88%.

intermediate 3-(3,4-dichlorophenyl)-5-(1-methyl-1*H*-pyrrol-2-yl)-4,5-dihydro-1*H*-pyrazole-1-carbothioamide **5** was obtained by heating to reflux with Thiosemicarbazide in ethanol for 8 h in the presence of catalytic amounts of sodium hydroxide.

In order to gain a deeper understanding of the SARs of the thiazole derivatives, we incorporated various aromatic and heteroaromatic residues at position 4 of the thiazole ring. The synthesis of the target compounds **6a–e** were by reaction of the last the key intermediate **5** with the appropriate phenacyl bromide derivative in ethanol. On the other hand, the starting material **3** on reacting with diethyl azodicarboxylate in the presence of triphenyl phosphine provides pyrazole-1,2(3*H*)-dicarboxylate derivative **4** as depicted in Scheme 1. The structures of all the final products were verified using ^{1}H and ^{13}C NMR spectroscopy.

With more focus on studying the effect of different residues at position 4 of the thiazole ring, the suitable intermediate **7** was synthesized from the starting material **5** *via* the reaction with α-bromopyruvate. Subsequently, we used hydrazine hydrate under reflux conditions to obtain the hydrazide derivative **8**. Further, the last compound was reacted with cyanogen bromide to afford the aminooxadiazole derivative **9**. Moreover, **8** reacted with aryl sulfonyl chloride derivatives to afford the corresponding benzene sulfonohydrazide derivatives **10a–c**, as outlined in Scheme 2.

Starting from the key intermediate **5**, we also decided to study incorporating the thiazolone ring and its derivatives at position 1 of the 1*H*-pyrazole ring. To begin, we synthesized the thiazolone derivative **11** through a reaction between **5** and ethyl bromoacetate in ethanol. Subsequently, to explore the

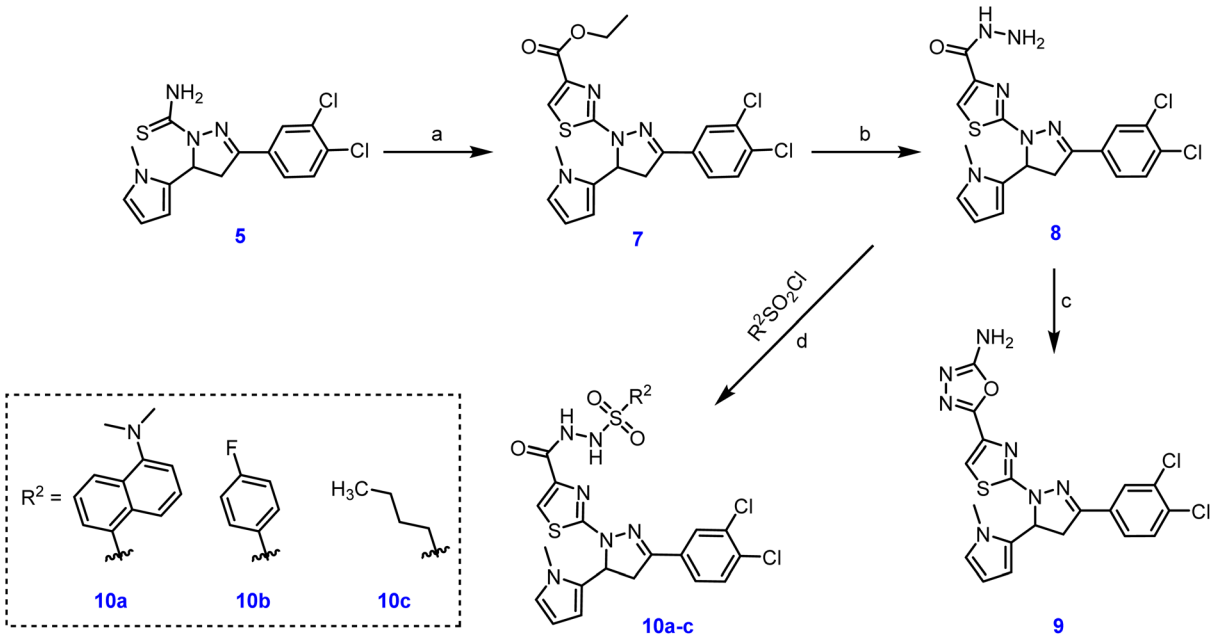

Scheme 2 Synthesis of target compounds **9**, and **10a–c**. Reagents and conditions: (a) α-bromopyruvate, EtOH, 60 °C, 4 h, 88%; (b) hydrazine hydrate, EtOH, 100 °C, 5h, 89%; (c) (1) cyanogen bromide, MeOH, 1,4-dioxane, rt, 1 h (2) $NaHCO_3$, rt, 18 h, 73%; (d) aryl sulfonyl chloride, DMF, 0 °C–rt, 4–10 h, 65–84%.

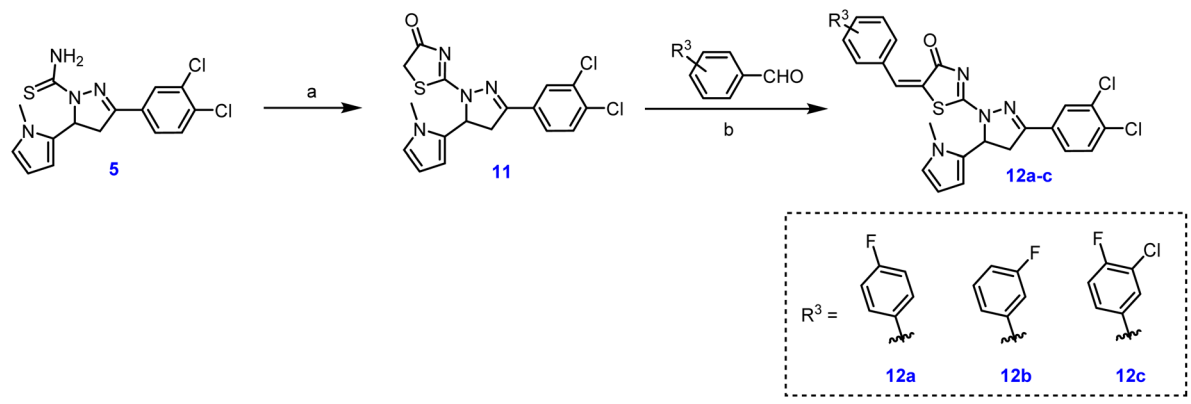

Scheme 3 Synthesis of target compounds **12a–c**. Reagents and conditions: (a) ethyl bromoacetate, EtOH, 100 °C, 3 h, 83%; (b) benzaldehyde derivative, piperidine, EtOH, 100 °C, 4 h, 71–81%.

derivatization at the thiazolone ring, we employed various aldehydes and condensed them with **11** in the presence of piperidine in ethanol to afford the target compounds 2-amino-5-benzylidenethiazol-4-one derivatives **12a–c**, as outlined in Scheme 3.

Biological screening

Cytotoxicity studies on cancer monolayers. Cytotoxicity studies were conducted on human cancer cell lines through the MTT assay. This assay is a pivotal component of cancer research and drug development that allows researchers to assess the potential toxicity of various compounds or treatments on cancer cells. The cytotoxic activity of our newly synthesized analogs was investigated on three cancer cell lines: human prostate cancer (PC-3), human breast cancer (MCF-7) and human lung cancer (A549) using *in vitro* MTT assay (Table 1).

The newly developed pyrazole derivatives demonstrated notable cytotoxic effects on the PC3, MCF-7 and A549 cancer cell lines highlighting their potential as anticancer agents. Specifically, compounds **4**, **5**, **6b**, **6c**, **7**, **8**, **10b**, **10c**, and **12b** demonstrated significant cytotoxic effects on the MCF-7 breast cancer cell line. Against the PC-3 cell line, compounds **5**, **7**, **10b**, and **10c** demonstrated significant cytotoxic effects. For the A549 lung cancer cell line, compounds **4**, **5**, **6b**, **7**, **10b**, **10c**, and **12b** showed significant cytotoxicity. The consistent presence of a chlorophenyl group in all compounds significantly contributes to their baseline cytotoxicity due to its strong electron-withdrawing properties (Fig. 3).

Compounds featuring a thiazole ring, such as **6c**, **8**, **10b**, and **10c**, exhibit enhanced cytotoxic activity. Additional ring systems like the pyridine ring in **6c** and the acylhydrazone group in **8** further boost the bonding interactions, respectively. Sulfonamide groups with substituents, particularly the fluorophenyl group in **10b** and the aliphatic chain in **10c**, significantly enhance cytotoxic effects, with **10c** showing the highest activity against MCF-7 cells.

The variation in IC_{50} values across different compounds indicates that specific structural modifications can significantly influence their anticancer activity. This variability underscores

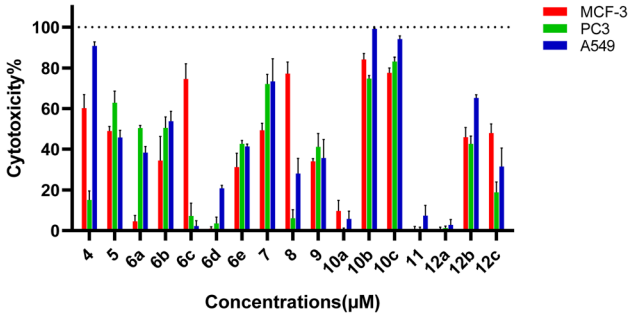

Fig. 3 Cytotoxicity% of our compounds against human prostate cancer (PC-3), human breast cancer (MCF-7) and human lung cancer (A549) at 100 μM concentration. Results are represented as the mean of three independent experiments ($n = 3$).

Table 1 The IC_{50} values for the most potent compounds against the PC-3, MCF-7 and A549 cancer cell lines. Results are represented as the mean of three independent experiments ($n = 3$)

	IC_{50} (μM)		
Compound	MCF-7	PC3	A549
4	67.8 ± 0.12	90.8 ± 0.166	28.4 ± 0.08
5	94.3 ± 0.122	81.0 ± 0.139	92.1 ± 0.112
6b	96.1 ± 0.135	91.2 ± 0.144	84.0 ± 0.14
6c	58.5 ± 0.10	95.3 ± 0.175	92.3 ± 0.184
7	92.3 ± 0.184	40.2 ± 0.110	44.4 ± 0.09
8	54.8 ± 0.09	92.1 ± 0.132	90.3 ± 0.155
10b	41.4 ± 0.08	62.2 ± 0.132	30.0 ± 0.10
10c	34.5 ± 0.157	54.1 ± 0.128	38.9 ± 0.10
12b	86.1 ± 0.145	95.4 ± 0.155	66.3 ± 0.10
Doxorubicin	45.02 ± 1.60	32.4 ± 0.70	35.4 ± 0.90

the importance of understanding the SAR to optimize these compounds for better efficacy. Against the PC-3 cell line, **7** showed the highest cytotoxicity with an IC_{50} of 40.2 ± 0.110 μM, followed by **10c** with 54.1 ± 0.128 μM and **10b** with 62.2 ± 0.132 μM. Compound **5** displayed the lowest activity with an IC_{50} of 81.0 ± 0.139 μM, reinforcing the need for potent substituents to enhance efficacy. Against the MCF-7 breast cancer cell line, the IC_{50} values of the compounds ranged widely, reflecting the impact of different structural features. Compound **10c** showed the highest cytotoxicity with an IC_{50} value of 34.5 ± 0.157 μM which is better than the reference compound doxorubicin with an IC_{50} vale of 45.02 ± 1.60 μM, indicating that the presence of a sulfonamide group with an aliphatic chain substantially enhances activity. **10b** also displayed significant activity with an IC_{50} of 41.4 ± 0.08 μM, attributed to its sulfonamide group with a fluorophenyl substituent.

Moderate activity was observed for **6c** and **8**, with IC_{50} values of 58.5 ± 0.10 μM and 54.8 ± 0.09 μM, respectively, highlighting the beneficial effects of the acylhydrazone and pyridine ring systems. Compound **5** exhibited the lowest activity against MCF-7, with an IC_{50} of 96.1 ± 0.135 μM, suggesting that additional potent substituents are necessary to enhance efficacy. For the A549 lung cancer cell line, the compounds also displayed varied cytotoxic effects. Compound **4** demonstrated the highest activity with an IC_{50} value of 28.4 ± 0.08 μM, indicating that the ester groups significantly improve the activity. **10b** showed strong activity with an IC_{50} of 30.0 ± 0.10 μM, likely due to the presence of the sulfonamide group with a fluorophenyl substituent. **10c** had an IC_{50} value of 38.9 ± 0.10 μM, suggesting that the aliphatic chain on the sulfonamide group enhances cytotoxicity. Compound **5** exhibited the lowest activity against A549, with an IC_{50} of 92.1 ± 0.112 μM.

Gene expression in cancer cell lines. The expression analysis of Bcl-2, BAX, P53, and Caspase-3 genes in three cancer cell lines (MCF-7, A549, and PC3) treated with compounds **6c**, **8**, **10b**, and **10c**, compared to the positive control doxorubicin, is detailed in Fig. 4. The results indicate a significant decrease in the expression levels of the anti-apoptotic gene Bcl-2 in all three cancer cell lines treated with our compounds, suggesting their potential as effective anticancer agents through the inhibition of Bcl-2 gene expression. Compound **6c** exhibited the most

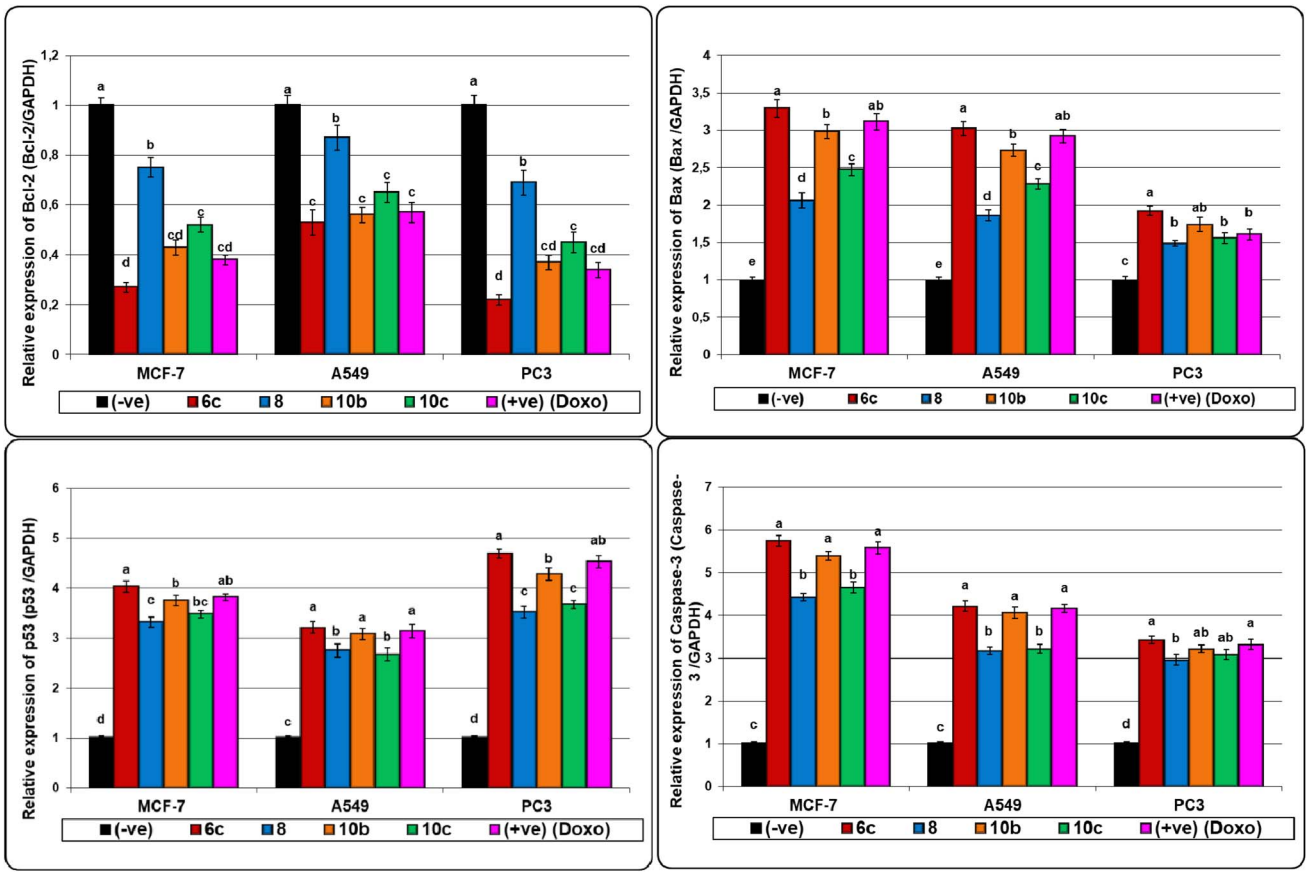

Fig. 4 The alterations of Bcl-2, BAX, P53, and Caspase-3 gene expression in three different cancer cell lines (MCF-7, A549 and PC3) treated with compounds **6c**, **8**, **10b**, **10c** and doxorubicin (Doxo). Data are presented as mean ± SEM. [a,b,c,d] Mean values within tissue with unlike superscript letters were significantly different ($P < 0.05$).

substantial decrease in Bcl-2 expression, surpassing the effect observed with doxorubicin. Notably, compounds **10b** and **10c** also showed a promising reduction in Bcl-2 expression across all three cancer cell lines.

Bcl-2 is known to prevent apoptosis by inhibiting the release of cytochrome c from mitochondria, thereby blocking the apoptotic cascade. The observed downregulation of Bcl-2 implies that our compounds can disrupt this protective mechanism, making cancer cells more susceptible to programmed cell death. This is particularly significant as overexpression of Bcl-2 is often associated with resistance to chemotherapy and poor prognosis in various cancers. In contrast, the expression levels of the pro-apoptotic genes BAX, p53, and Caspase-3 increased significantly in the treated cancer cell lines. Compounds **6c**, **10b**, and **10c** demonstrated a promising increase in the expression of these pro-apoptotic genes when compared to Doxorubicin. Specifically, these compounds enhanced the expression of BAX and Caspase-3 in MCF-7 and A549 cancer cell lines, with a slightly lesser effect observed in the PC3 cells. This suggests that these compounds can trigger apoptosis more effectively in breast and lung cancer cells.

BAX promotes apoptosis by promoting the release of cytochrome c from the mitochondria, leading to the activation of caspases. Caspase-3 is a critical executioner of apoptosis, responsible for the cleavage of various cellular substrates leading to cell death. The increased expression of these genes suggests that our compounds can effectively initiate and propagate the apoptotic signal within cancer cells. Regarding p53, the highest increase in gene expression was observed in PC3 cells. p53, often referred to as the "guardian of the genome," plays a crucial role in regulating the cell cycle and inducing apoptosis in response to DNA damage. The upregulation of p53 indicates that our compounds may enhance the DNA damage response, leading to increased cell cycle arrest and apoptosis in prostate cancer cells.

The differential effects of our compounds on various cell lines underscore the complexity of their action mechanisms. While all compounds were effective in downregulating BCL-2 and upregulating BAX, p53, and Caspase-3, the extent of these effects varied among the cell lines. This variability suggests that the efficacy of our compounds may depend on the specific genetic and molecular context of each cancer type. These findings highlight the potential of compounds **6c**, **10b**, and **10c** as powerful anticancer agents capable of modulating key apoptotic pathways. Their ability to decrease BCL-2 and increase BAX, p53, and Caspase-3 expression provides a strong rationale for further investigation and development of these compounds as targeted therapies for cancer treatment. Future studies should

focus on elucidating the precise molecular interactions and pathways involved, as well as evaluating the *in vivo* efficacy and safety of these compounds in animal models.

DNA damage in cancer cell lines using comet assay. The DNA damage in three cancer cell lines (MCF-7, A549, and PC3) was determined using the comet assay, a sensitive and rapid technique for measuring DNA strand breaks in individual cells. This assay involves embedding cells in agarose, lysing them to release DNA, subjecting them to electrophoresis, and staining the DNA to visualize the extent of damage, which appears as a 'comet tail' extending from the nucleus. The length and intensity of the tail relative to the head indicate the level of DNA damage. As shown in Tables S1–S3 in the ESI,† DNA damage values significantly increased ($P < 0.01$) in the three cancer cell lines treated with our novel pyrazolo derivatives (**6c**, **8**, **10b**, and **10c**). These compounds demonstrated high DNA damage percentages (>20%), comparable to that of the well-known anticancer drug doxorubicin. This indicates that our compounds have promising cytotoxic effects on MCF-7, A549, and PC3 cancer cell lines.

Compounds **6c**, **8**, **10b**, and **10c** induced substantial DNA damage, as evidenced by the increased comet tail length and percentage of DNA in the tail. The presence of DNA strand breaks, as visualized by the comet assay, suggests that these compounds effectively induce genotoxic stress in cancer cells. This genotoxicity is a critical aspect of their anticancer activity, leading to apoptosis and cell death. In detail, the DNA damage induced by compound **6c** was the most pronounced, with values surpassing those observed with Doxorubicin. This suggests that compound **6c** is particularly effective in causing DNA strand breaks, thereby triggering cell death pathways. Similarly, compounds **10b** and **10c** also showed significant DNA damage, indicating their potential as strong anticancer agents. Compound **8**, while slightly less effective than **6c**, still demonstrated considerable DNA damage, supporting its role in cancer cell cytotoxicity. The comet assay results highlight the mechanism by which our compounds exert their anticancer effects. By causing significant DNA damage, they likely activate the DNA damage response pathways, leading to cell cycle arrest and apoptosis. This mechanism is supported by the observed increase in pro-apoptotic gene expression (BAX, p53, and Caspase-3) and the decrease in the anti-apoptotic gene Bcl-2, as discussed previously.

Molecular docking studies

Compounds **6c**, **8**, **10b**, and **10c**, among the newly synthesized 1,3,5-trisubstituted-1*H*-pyrazole derivatives, showed the highest cytotoxic activities towards MCF-7, A549, and PC3 cancer cell lines. These compounds significantly decreased Bcl-2 gene expression while increasing the expression of pro-apoptotic genes Bax, P53, and Caspase-3. This implies their anticancer mechanism may involve disrupting Bcl-2's interactions with pro-apoptotic and autophagy-related proteins. Based on these observations, we used molecular docking to study the binding affinities and interactions of these compounds with the Bcl-2 protein.

The X-ray crystallographic structure of the Bcl-2 protein, along with its native ligand phenylacyl sulfonamide derivative (*N*,*N*-dibutyl-4-chloranyl-1-[2-(3,4-dihydro-1*H*-isoquinolin-2-ylcarbonyl) -4-[(7-iodanylnaphthalen-2-yl)sulfonylcarbamoyl] phenyl]-5-methyl-pyrazole-3-carboxamide), was obtained from the Protein Data Bank (PDB) under the accession code 4AQ3. The receptor preparation for docking was carried out using Biovia Discovery Studio. Initially, all water molecules and non-essential chains were removed from the protein structure to avoid any interference during the docking process. Polar hydrogen atoms were then added to the protein to accurately simulate hydrogen bonding interactions.

Subsequently, partial charges were adjusted to ensure proper electrostatic interactions within the protein structure. Energy minimization was performed to optimize the protein conformation, ensuring a stable and realistic receptor model. This

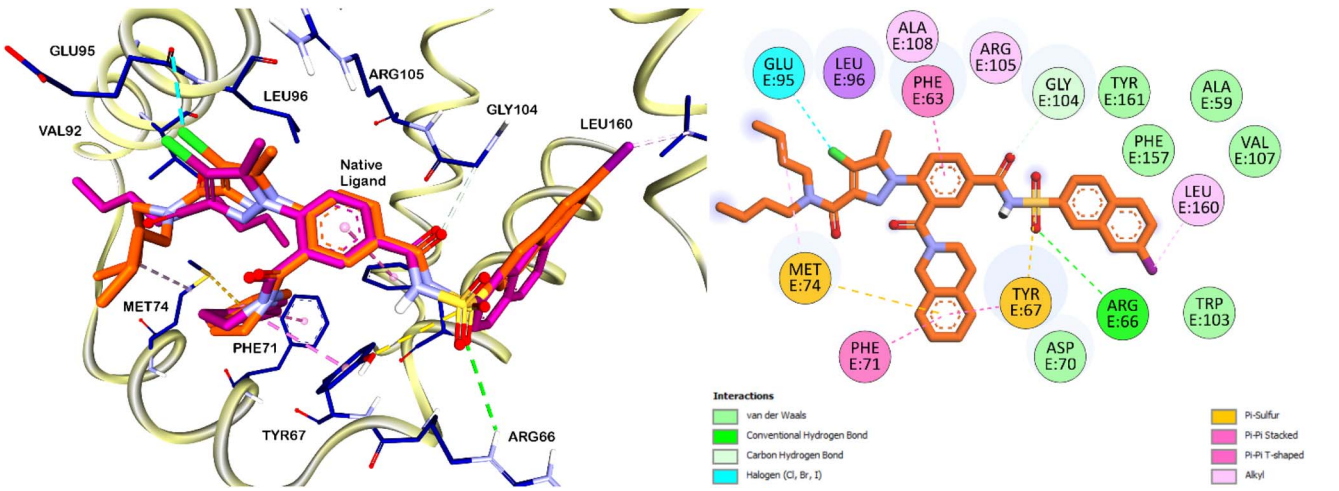

Fig. 5 (A) Superimposition of the naturally co-crystallized phenylacyl sulfonamide native ligand with the docked one within the active site of Bcl-2 protein (PDB ID: 4AQ3). The carbon atoms of the original ligand are depicted in violet, while those of the docked ligand are represented in orange; (B) 2D interactions between the docked ligand and Bcl-2 protein.

meticulous preparation of the Bcl-2 protein was crucial for achieving accurate and reliable docking simulations, which were conducted using the Autodock 4.2 software package. The validation phase of the docking software began with the redocking of the native ligand into the Bcl-2 protein's binding pocket. This process yielded an RMSD (Root Mean Square Deviation) value of 0.75 Å, reflecting a high degree of accuracy in reproducing the native ligand's position. Furthermore, the redocked ligand displayed a binding free energy (ΔG) of -14.55 kcal mol^{-1} (Fig. 5). According to the interactions documented by Perez H. L. *et al.*, the sulfonamide moiety of the native ligand engages in critical interactions with the ARG66 and TYR67 residues. Remarkably, our compounds **10b** and **10c**, which also feature a sulfonamide core, exhibited similar interactions (Fig. 6 and 7). This observation suggests that the sulfonamide group contributes to the stabilization of these compounds within the Bcl-2 protein pocket, enhancing their binding affinity.

In analogy to the observed halogen-bond interaction of the chloro group in the pyrazole moiety of the native ligand with GLU95 residue (Fig. 5), the chloro group on the terminal phenyl ring of compound **10c** (Fig. 7) displayed a similar interaction. This specific interaction type is crucial within protein binding sites, as it can contribute significantly to the stability and specificity of ligand–protein interactions. The similarity in binding interactions observed with our compounds and the native ligand, particularly through halogen bonding with GLU95, underscores the structural mimicry and potential efficacy of our compounds in targeting the Bcl-2 protein.

The phenyl ring of the native ligand is engaged in a pi–pi stacked hydrophobic interaction with the PHE63 residue, highlighting its aromatic interactions within the binding pocket. Additionally, the isoquinoline moiety formed pi–pi T-shaped interactions with the PHE71 residue and Pi-sulfur interactions with the MET74 residue (Fig. 5). Similarly, the terminal phenyl ring of compound **10b** also participates in pi–pi

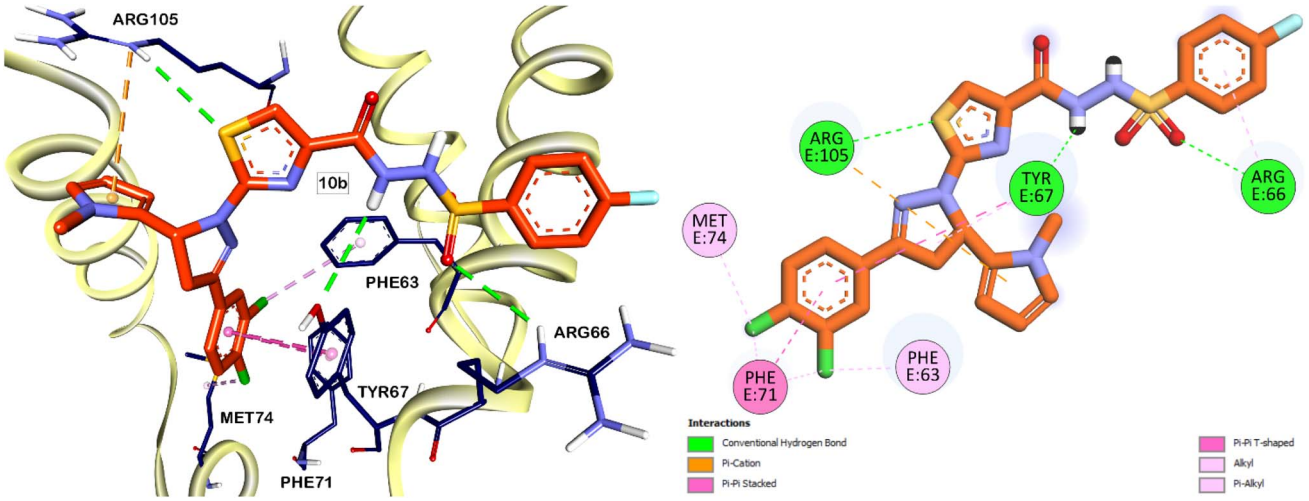

Fig. 6 Predicted binding interactions (3D and 2D) of compound **10b** within the active site of Bcl-2 protein. The carbon atoms of compound **10b** are colored in orange.

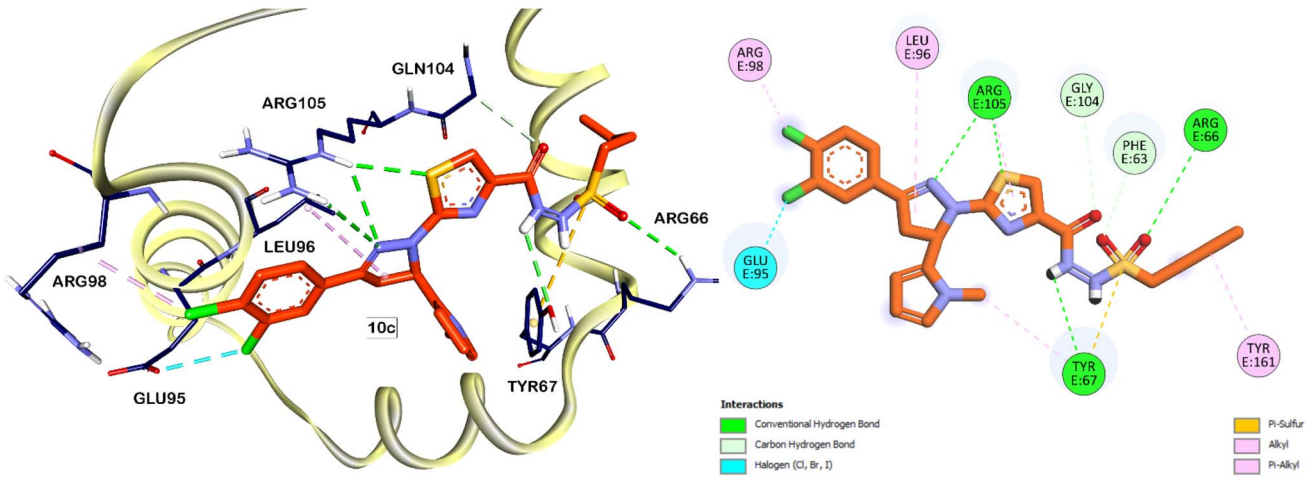

Fig. 7 Predicted binding interactions (3D and 2D) of compound **10c** within the active site of Bcl-2 protein. The carbon atoms of compound **10c** are colored in orange.

stacked and pi–pi T-shaped hydrophobic interactions with the PHE71 residue. These interactions play a crucial role in stabilizing the ligand within the binding site of the Bcl-2 protein, thereby enhancing its overall binding affinity and specificity. In addition to the previously mentioned interactions, the sulphur atom of the thiazole ring in compounds **10b** and **10c** is involved with H-bonding with ARG105 residue. This interaction was not observed with the native ligand which have a phenyl ring instead of the thiazole ring in its core, therefore, having heterocycle in this position would contribute to improved affinities of the Bcl-2 inhibitors.

Conclusion

In conclusion, the pursuit of novel anticancer agents targeting apoptotic and autophagic pathways is of paramount importance due to their critical roles in maintaining cellular homeostasis and eradicating cancer cells. In this study, a comprehensive exploration was conducted on a series of 1,3,5-trisubstituted-1*H*-pyrazole derivatives designed as potential inhibitors of the Bcl-2 protein, a pivotal regulator of apoptosis and autophagy. Our investigation revealed that several compounds exhibited significant cytotoxicity against MCF-7, A549, and PC-3 cancer cell lines, with notable potency observed in compounds **10b** and **10c**. These compounds demonstrated robust binding affinity to Bcl-2 and effectively activated pro-apoptotic proteins including Bax, p53, and Caspase-3. The structural–activity relationship (SAR) analysis highlighted the importance of chlorophenyl groups, thiazole rings, and sulfonamide substituents in enhancing cytotoxic effects. Molecular docking studies provided further insights, confirming strong hydrogen bonding interactions for compounds **10b** and **10c** with the Bcl-2 protein. Overall, these findings underscore the promising potential of our synthesized derivatives as effective anticancer agents, warranting continued investigation for future therapeutic applications in oncology.

Experimental

Chemistry

All chemicals and solvents were sourced from Acros, BLD, TCI, Aldrich, Fluka, Merck, and Sigma, and were used as received without further purification. Analytical and spectral analyses of the synthesized compounds were performed at the Microanalytical Labs of the National Research Centre and the Microanalytical Laboratory Center at the Faculty of Science, Cairo University, Egypt. ^{1}H and ^{13}C Nuclear Magnetic Resonance (NMR) spectra were obtained on Joel ECA 500 MHz spectrometers, using DMSO-d_6 as the solvent. Chemical shifts are reported in parts per million (ppm) relative to the tetramethylsilane (TMS) standard in the solvent. Coupling constants are expressed in Hertz (Hz). The abbreviations for the splitting patterns are: singlet (s), doublet (d), triplet (t), and multiplet (m). Melting points were measured using a Stuart SMP30 Melting Point Apparatus and are uncorrected. Reaction progress was monitored *via* thin layer chromatography (TLC) using Merck Silica Gel 60 F254 plates.

(*E*)-1-(3,4-dichlorophenyl)-3-(1-methyl-1*H*-pyrrol-2-yl)prop-2-en-1-one (3). A solution of 3′,4′-dichloroacetophenone (2.00 g, 10.58 mmol) in EtOH (20 mL) was prepared and stirred at 0 °C. To this solution, 6.0 mL of 10% aqueous NaOH was added. After stirring for 0.5 h, a solution of 1-methyl-1*H*-imidazole-5-carbaldehyde (1.15 g, 10.58 mmol) in EtOH was added. The reaction mixture was stirred until completion (4 h, monitored by TLC). The resulting mixture was added to ice water, and the formed precipitate was filtered and washed with cold methanol to yield compound **3** as a yellow solid (2.39 g, 81%). ^{1}H NMR (600 MHz, DMSO-d_6) δ 8.32 (d, J = 2.0 Hz, 1H, CH=*CH*), 8.07 (dd, J = 8.4, 2.1 Hz, 1H, *CH*=CH), 7.86 (s, 2H, Ar-H), 7.83 (d, J = 8.4 Hz, 1H, Ar-H), 7.74–7.64 (m, 2H, Ar-H), 3.80 (s, 3H, NCH_3). ^{13}C NMR (151 MHz, DMSO-d_6) δ 186.32, 142.38, 137.81, 135.76, 134.03, 131.89, 131.07, 130.68, 130.10, 129.18, 128.32, 117.94, 31.75. HPLC-UV (254 nm) for $C_{14}H_{11}Cl_2NO$ ESI-MS, purity: 96.5%. LC-MS (m/z): 280.10 $[M + H]^+$.

Diethyl 5-(3,4-dichlorophenyl)-3-(1-methyl-1*H*-pyrrol-2-yl)-1*H*-pyrazole-1,2(3*H*)-dicarboxylate (4). To a solution of chalcone **3** (0.10 g, 0.36 mmol) in toluene (2.0 mL), diethyl azodicarboxylates (0.09 g, 0.54 mmol) was added followed by the addition of Ph_3P (0.09 g, 0.36 mmol), and the reaction mixture was stirred at room temperature for 7 h. Then the mixture was directly purified by flash column chromatography on a silica gel to afford the corresponding product **4** (0.08 g, 60%). ^{1}H NMR (600 MHz, DMSO-d_6) δ 7.78 (d, J = 2.1 Hz, 1H), 7.68 (d, J = 8.4 Hz, 1H, Ar-H), 6.76 (dd, J = 2.6, 1.9 Hz, 1H), 6.37 (d, J = 3.3 Hz, 1H, Ar-H), 5.97 (d, J = 3.3 Hz, 1H, Ar-H), 5.89 (dd, J = 3.6, 2.6 Hz, 1H), 5.87 (dd, J = 3.7, 1.8 Hz, 1H), 4.22 (qq, J = 7.2, 3.5 Hz, 2H), 4.00–3.88 (m, 2H), 3.71 (s, 3H), 1.25 (t, J = 7.1 Hz, 3H), 0.89 (t, J = 7.1 Hz, 3H). ^{13}C NMR (151 MHz, DMSO-d_6) δ 155.82, 141.03, 133.26, 132.18, 132.16, 131.67, 131.60, 131.12, 130.56, 128.86, 128.49, 127.20, 124.21, 115.01, 108.51, 62.67, 62.44, 33.74, 14.44, 14.01. HPLC-UV (254 nm) for $C_{20}H_{21}Cl_2N_3O_4$ ESI-MS, purity: 97.3%. LC-MS (m/z): 438.12 $[M + H]^+$.

3-(3,4-Dichlorophenyl)-5-(1-methyl-1*H*-pyrrol-2-yl)-4,5-dihydro-1*H*-pyrazole-1-carbothio-amide (5). A mixture of chalcone **3** (1.00 g, 3.57 mmol) and NaOH (0.356 g, 7.26 mmol) in 20 mL of ethanol was stirred vigorously under reflux with thiosemicarbazide (0.324 g, 3.57 mmol) for 8 h. The resulting mixture was then cooled and the desired product was obtained as a white precipitate. The precipitate was filtered under vacuum, then recrystallized from ethanol and dried, yielding a white solid product of **5** in a yield of (1.09 g, 87%). ^{1}H NMR (600 MHz, DMSO-d_6) δ 8.22 (d, J = 2.0 Hz, 1H), 8.04 (d, J = 18.6 Hz, 2H), 7.80 (dd, J = 8.3, 2.0 Hz, 1H), 7.72 (d, J = 8.4 Hz, 1H), 6.57 (dd, J = 2.6, 1.9 Hz, 1H), 5.91 (dd, J = 11.4, 3.6 Hz, 1H), 5.83 (dd, J = 3.6, 2.6 Hz, 1H), 5.62 (dd, J = 3.7, 1.8 Hz, 1H), 3.77 (dd, J = 17.9, 11.4 Hz, 1H), 3.67 (s, 3H), 3.23 (dd, J = 17.9, 3.6 Hz, 1H). ^{13}C NMR (151 MHz, DMSO-d_6) δ 176.52, 152.85, 133.69, 132.93, 132.12, 132.00, 131.12, 128.78, 127.34, 121.70, 106.68, 104.51, 56.58, 41.53, 34.04. HPLC-UV (254 nm) for $C_{15}H_{14}Cl_2N_4S$ ESI-MS, purity: 98.3%. LC-MS (m/z): 353.10 $[M + H]^+$.

General procedure for the synthesis of compounds 6a–e

To a solution of pyrazol-1-ylthiocarboxamide **5** (0.05 g, 0.141 mmol) in 2 mL of ethanol, phenacyl bromide derivative (0.143

mmol) was added to the solution and then refluxed at 100 °C for 3 h. After cooling, the product was obtained by filtration, washed with cold ethanol, and dried. The resulting compound was recrystallized using hot ethanol to obtain the desired compounds **6a–e**.

4-(4-Chlorophenyl)-2-(3-(3,4-dichlorophenyl)-5-(1-methyl-1*H*-pyrrol-2-yl)-4,5-dihydro-1*H*-pyrazol-1-yl)thiazole (6a). Pyrazol-1-ylthiocarboxamide **5** (0.05 g, 0.141 mmol) was dissolved in 2 mL of ethanol. Then, 4-chlorophenacyl bromide (0.033 g, 0.143 mmol) was added to the solution and refluxed for 3 h. After cooling, the product **6a** was obtained by filtration, washed with cold ethanol, and dried. The resulting compound was recrystallized using hot ethanol, with a yield of (0.049 g, 72%). ^{1}H NMR (400 MHz, DMSO-d_6) δ 7.95 (d, J = 1.9 Hz, 1H), 7.80–7.75 (m, 4H), 7.49–7.40 (m, 3H), 6.67 (dd, J = 2.6, 1.8 Hz, 1H), 5.96 (dd, J = 3.7, 1.8 Hz, 1H), 5.90 (dd, J = 3.7, 2.7 Hz, 1H), 5.80 (dd, J = 12.0, 6.6 Hz, 1H), 3.94 (dd, J = 17.9, 12.1 Hz, 1H), 3.81 (s, 3H), 3.49 (dd, J = 17.9, 6.6 Hz, 1H). HPLC-UV (254 nm) for $C_{23}H_{17}Cl_3N_4S$ ESI-MS, purity: 96.3%. LC-MS (m/z): 487.22 $[M + H]^+$.

2-(3-(3,4-Dichlorophenyl)-5-(1-methyl-1*H*-pyrrol-2-yl)-4,5-dihydro-1*H*-pyrazol-1-yl)-4-(2-methoxyphenyl)thiazole (6b). Pyrazol-1-ylthiocarboxamide **5** (0.05 g, 0.141 mmol) was dissolved in 2 mL of ethanol. Then, 2-methoxyphenacyl bromide (0.033 g, 0.143 mmol) was added to the solution and refluxed for 3 h. After cooling, the product **6b** was obtained by filtration, washed with cold ethanol, and dried. The resulting compound was recrystallized using hot ethanol, with a yield of (0.04 g, 58%). ^{1}H NMR (400 MHz, DMSO-d_6) δ 7.94 (d, J = 1.9 Hz, 1H), 7.89 (dd, J = 7.7, 1.8 Hz, 1H), 7.80–7.71 (m, 2H), 7.40 (s, 1H), 7.27 (ddd, J = 8.6, 7.3, 1.8 Hz, 1H), 7.10–7.05 (m, 1H), 6.99 (td, J = 7.5, 1.1 Hz, 1H), 6.67 (t, J = 2.2 Hz, 1H), 5.96 (dd, J = 3.7, 1.8 Hz, 1H), 5.89 (dd, J = 3.6, 2.7 Hz, 1H), 5.79 (dd, J = 12.1, 6.8 Hz, 1H), 3.99–3.90 (m, 1H), 3.88 (s, 3H), 3.78 (s, 3H), 3.47 (dd, J = 18.0, 6.8 Hz, 1H). HPLC-UV (254 nm) for $C_{24}H_{20}Cl_2N_4OS$ ESI-MS, purity: 96.8%. LC-MS (m/z): 483.15 $[M + H]^+$.

2-(3-(3,4-Dichlorophenyl)-5-(1-methyl-1*H*-pyrrol-2-yl)-4,5-dihydro-1*H*-pyrazol-1-yl)-4-(pyridin-4-yl)thiazole (6c). Pyrazol-1-ylthiocarboxamide **5** (0.05 g, 0.141 mmol) was dissolved in 2 mL of ethanol. Then, 4-bromoacetylpyridine (0.028 g, 0.143 mmol) was added to the solution and refluxed for 3 h. After cooling, the product **6c** was obtained by filtration, washed with cold ethanol, and dried. The resulting compound was recrystallized using hot ethanol, with a yield of (0.054 g, 84%). ^{1}H NMR (500 MHz, DMSO-d_6) δ 8.90–8.84 (m, 2H), 8.26 (s, 1H), 8.24–8.20 (m, 2H), 7.99 (d, J = 2.0 Hz, 1H), 7.83–7.73 (m, 2H), 6.70 (t, J = 2.3 Hz, 1H), 6.00 (dd, J = 3.7, 1.9 Hz, 1H), 5.93–5.90 (m, 1H), 5.87 (dd, J = 12.0, 6.7 Hz, 1H), 4.01 (dd, J = 18.0, 12.0 Hz, 1H), 3.81 (s, 3H). HPLC-UV (254 nm) for $C_{22}H_{17}Cl_2N_5S$ ESI-MS, purity: 100%. LC-MS (m/z): 454.22 $[M + H]^+$.

4-(2-Chlorophenyl)-2-(3-(3,4-dichlorophenyl)-5-(1-methyl-1*H*-pyrrol-2-yl)-4,5-dihydro-1*H*-pyrazol-1-yl)thiazole (6d). Pyrazol-1-ylthiocarboxamide **5** (0.05 g, 0.141 mmol) was dissolved in 2 mL of ethanol. Then, 2-chlorophenacyl bromide (0.033 g, 0.143 mmol) was added to the solution and refluxed for 3 h. After cooling, the product **6d** was obtained by filtration, washed with cold ethanol, and dried. The resulting compound was recrystallized using hot ethanol, with a yield of (0.04 g, 88%). ^{1}H NMR (600 MHz, DMSO-d_6) δ 7.95 (s, 3H), 7.76 (d, J = 15.9 Hz, 3H), 7.70 (d, J = 9.5 Hz, 1H), 7.51 (s, 1H), 7.41–7.29 (m, 2H), 6.65 (s, 3H), 5.94 (s, 1H), 5.90 (s, 1H), 5.77 (d, J = 18.7 Hz, 1H), 3.95 (d, J = 30.0 Hz, 1H), 3.75 (s, 6H), 3.48 (d, J = 24.6 Hz, 1H). ^{13}C NMR (151 MHz, DMSO-d_6) δ 163.49, 150.80, 147.22, 133.18, 132.28, 131.95, 131.92, 131.82, 131.22, 131.17, 130.81, 130.51, 129.18, 128.05, 127.31, 126.37, 122.54, 109.94, 106.89, 106.62, 56.97, 42.00, 34.13. HPLC-UV (254 nm) for $C_{23}H_{17}Cl_3N_4S$ ESI-MS, purity: 100%. LC-MS (m/z): 485.30 $[M - H]^-$.

2-(3-(3,4-Dichlorophenyl)-5-(1-methyl-1*H*-pyrrol-2-yl)-4,5-dihydro-1*H*-pyrazol-1-yl)-4-(1-phenyl-1*H*-pyrazol-4-yl)thiazole (6e). Pyrazol-1-ylthiocarboxamide **5** (0.05 g, 0.141 mmol) was dissolved in 2 mL of ethanol. Then, 2-bromo-1-(1-phenyl-1*H*-pyrazol-4-yl)ethanone (0.038 g, 0.143 mmol) was added to the solution and refluxed for 3 h. After cooling, the product **6c** was obtained by filtration, washed with cold ethanol, and dried. The resulting compound was recrystallized using hot ethanol, with a yield of (0.036 g, 49%). ^{1}H NMR (400 MHz, DMSO-d_6) δ 7.94 (d, J = 1.9 Hz, 1H), 7.86 (s, 1H), 7.79–7.72 (m, 1H), 7.58–7.49 (m, 4H), 7.48–7.40 (m, 1H), 6.93 (s, 1H), 6.65 (dd, J = 2.7, 1.8 Hz, 1H), 5.94 (dd, J = 3.6, 1.8 Hz, 1H), 5.88 (dd, J = 3.7, 2.6 Hz, 1H), 5.76 (dd, J = 12.1, 7.1 Hz, 1H), 3.93 (dd, J = 17.9, 12.2 Hz, 1H), 3.73 (s, 3H), 3.44 (dd, J = 18.0, 7.1 Hz, 1H), 2.37 (s, 3H). HPLC-UV (254 nm) for $C_{26}H_{20}Cl_2N_6S$ ESI-MS, purity: 100%. LC-MS (m/z): 517.29 $[M - H]^-$.

Ethyl 2-(3-(3,4-dichlorophenyl)-5-(1-methyl-1*H*-pyrrol-2-yl)-4,5-dihydro-1*H*-pyrazol-1-yl)thiazole-4-carboxylate (7). The compound **5** (2.0 g, 5.68 mmol) and α-bromopyruvate (1.11 g, 5.68 mmol), were dissolved in ethanol and subjected to vigorous stirring at 60 °C for 4 h. The resulting ethyl thiazole-4-carboxylate derivative was precipitated, filtered, and washed with ethanol to obtain a solid mass. This solid was then recrystallized from ethanol to yield **7** (2.23 g, 88%) as a yellow solid. ^{1}H NMR (600 MHz, DMSO-d_6) δ 7.95 (d, J = 2.0 Hz, 1H), 7.79–7.71 (m, 3H), 6.63 (dd, J = 2.6, 1.8 Hz, 1H), 5.91–5.85 (m, 2H), 5.73 (dd, J = 11.9, 6.1 Hz, 1H), 4.22 (q, J = 7.1 Hz, 2H), 3.90 (s, 3H), 3.50 (dd, J = 17.9, 6.1 Hz, 1H), 1.27 (t, J = 7.1 Hz, 3H). ^{13}C NMR (151 MHz, DMSO-d_6) δ 164.33, 160.99, 151.53, 142.98, 132.47, 131.94, 131.88, 131.77, 131.24, 128.19, 126.46, 122.62, 120.28, 106.90, 106.38, 60.58, 56.55, 42.31, 34.21, 14.27. HPLC-UV (254 nm) for $C_{20}H_{18}Cl_2N_4O_2S$ ESI-MS, purity: 95.2%. LC-MS (m/z): 449.18 $[M + H]^+$.

2-(3-(3,4-Dichlorophenyl)-5-(1-methyl-1*H*-pyrrol-2-yl)-4,5-dihydro-1*H*-pyrazol-1-yl)thiazol -4-carbohydrazide (8). Compound **7** (2.0 g, 4.45 mmol) was mixed with hydrazine hydrate (0.8 mL) in absolute ethanol (20 mL) and heated under reflux for 5 h. After cooling, the resulting crystalline material was recrystallized from ethanol, yielding the title product **8** (1.73 g, 89%). ^{1}H NMR (500 MHz, DMSO-d_6) δ 8.70 (s, 1H), 7.94 (d, J = 2.0 Hz, 1H), 7.81–7.68 (m, 2H), 7.49 (s, 1H), 6.66 (t, J = 2.3 Hz, 1H), 5.95–5.83 (m, 2H), 5.78 (dd, J = 11.9, 5.9 Hz, 1H), 4.47 (s, 2H), 3.93 (dd, J = 17.9, 11.9 Hz, 1H), 3.74 (s, 3H), 3.47 (dd, J = 17.9, 5.9 Hz, 1H). ^{13}C NMR (126 MHz, DMSO-d_6) δ 164.30, 160.58, 151.59, 145.40, 132.48, 131.93, 131.77, 131.31, 131.24, 128.18, 126.44, 122.88, 114.02, 106.79, 106.71, 57.19,

41.72, 34.13. HPLC-UV (254 nm) for $C_{18}H_{16}Cl_2N_6OS$ ESI-MS, purity: 96.7%. LC-MS (*m*/*z*): 435.12 $[M + H]^+$.

5-(2-(3-(3,4-Dichlorophenyl)-5-(1-methyl-1*H*-pyrrol-2-yl)-4,5-dihydro-1*H*-pyrazol-1-yl)thiazol-4-yl)-1,3,4-oxadiazol-2-amine (9). A solution of **8** (0.10 g, 0.23 mmol) in MeOH (4 mL) and 1,4-dioxane (2 mL) was mixed with BrCN (0.17 mL, 3 M solution in CH_2Cl_2) gradually at room temperature. After stirring for an hour, 0.08 g $NaHCO_3$ was added to the mixture and the resulting suspension was stirred for 18 h. The white precipitate that formed was filtered, washed with water and dried under high vacuum. The yield was (77 mg, 73%) of **9** as a white solid that was recrystallized from ethanol. ^{1}H NMR (500 MHz, DMSO-d_6) δ 7.96 (d, J = 2.0 Hz, 1H), 7.83–7.71 (m, 2H), 7.39 (s, 1H), 7.18 (s, 2H), 6.65 (t, J = 2.3 Hz, 1H), 5.88 (q, J = 3.6, 2.6 Hz, 2H), 5.79 (dd, J = 11.9, 5.8 Hz, 1H), 3.96 (dd, J = 18.0, 11.9 Hz, 1H), 3.90 (s, 2H), 3.57 (s, 3H), 3.51 (dd, J = 17.9, 5.8 Hz, 1H). ^{13}C NMR (126 MHz, DMSO-d_6) δ 165.22, 163.45, 154.17, 151.66, 136.64, 132.48, 131.92, 131.78, 131.72, 131.22, 128.18, 126.45, 122.64, 111.03, 106.87, 106.29, 66.48, 56.67, 42.26, 34.23. HPLC-UV (254 nm) for $C_{19}H_{15}Cl_2N_7OS$ ESI-MS, purity: 98.1%. LC-MS (*m*/*z*): 460.15 $[M + H]^+$.

General procedure for the synthesis of compounds 10a–c

To a solution of acid hydrazide **8** (100 mg, 0.23 mmol) in DMF (10 mL) and cooled to 0 °C, sulfonyl chloride derivative (0.23 mmol) was added portion wise and then the reaction mixture was stirred at room temperature for 4 h. When the reaction is finished, distilled water (25 mL) was added and the formed precipitate that formed was filtered, washed with water and dried under high vacuum. The formed precipitate was recrystallized from ethanol yielding compounds **10a–c**.

***N*′-(2-(3-(3,4-Dichlorophenyl)-5-(1-methyl-1*H*-pyrrol-2-yl)-4,5-dihydro-1*H*-pyrazol-1-yl)thiazole-4-carbonyl)-5-(dimethylamino) naphthalene-1-sulfonohydrazide (10a).** To a solution of acid hydrazide **8** (100 mg, 0.23 mmol) in DMF (10 mL) and cooled to 0 °C, dansyl chloride (62 mg, 0.23 mmol) was added portionwise and then the reaction mixture was stirred at room temperature for 4 h. When the reaction is finished, distilled water (25 mL) was added and the formed precipitate that formed was filtered, washed with water and dried under high vacuum. The precipitate was recrystallized from ethanol yielding **10a** (128 mg, 84%) of as yellow solid. ^{1}H NMR (500 MHz, DMSO-d_6) δ 10.18 (d, J = 2.4 Hz, 1H), 9.43 (d, J = 2.3 Hz, 1H), 8.50 (d, J = 8.5 Hz, 1H), 8.37 (d, J = 8.6 Hz, 1H), 8.21–8.14 (m, 1H), 7.94 (d, J = 1.9 Hz, 1H), 7.80–7.71 (m, 3H), 7.57 (ddd, J = 22.1, 8.7, 7.5 Hz, 2H), 7.46 (s, 1H), 7.27 (d, J = 7.5 Hz, 1H), 6.52 (t, J = 2.2 Hz, 1H), 5.79 (dq, J = 6.2, 3.6 Hz, 2H), 5.68 (dd, J = 11.9, 6.1 Hz, 1H), 3.96–3.86 (m, 2H), 3.82–3.72 (m, 1H), 3.63 (s, 3H), 3.51–3.44 (m, 1H), 2.93 (s, 1H), 2.84 (s, 6H). ^{13}C NMR (126 MHz, DMSO-d_6) δ 164.28, 159.99, 151.81, 151.15, 144.96, 144.62, 143.94, 134.97, 132.53, 131.94, 131.71, 131.29, 131.24, 130.53, 130.28, 129.87, 129.22, 128.20, 127.92, 126.47, 126.36, 125.37, 124.69, 124.41, 123.65, 122.65, 119.99, 116.21, 115.31, 106.87, 106.77, 56.92, 45.62, 45.29, 41.75, 34.09. HPLC-UV (254 nm) for $C_{30}H_{27}Cl_2N_7O_3S_2$ ESI-MS, purity: 97.5%. LC-MS (*m*/*z*): 668.23 $[M + H]^+$.

***N*′-(2-(3-(3,4-Dichlorophenyl)-5-(1-methyl-1*H*-pyrrol-2-yl)-4,5-dihydro-1*H*-pyrazol-1-yl)thiazole-4-carbonyl)-4-fluorobenzenesulfonohydrazide (10b).** To a solution of **8** (100 mg, 0.23 mmol) in DMF (10 mL) and cooled to 0 °C, 4-fluorobenzenesulfonyl chloride (45 mg, 0.23 mmol) was added portionwise and then the reaction mixture was stirred at room temperature for 6 h. When the reaction is finished, distilled water (25 mL) was added and the formed precipitate that formed was filtered, washed with water and dried under high vacuum. The formed precipitate was recrystallized from ethanol yielding **10b** (87 mg, 66%) of as buff solid. ^{1}H NMR (500 MHz, DMSO-d_6) δ 10.10 (d, J = 3.3 Hz, 1H), 9.71 (d, J = 3.2 Hz, 1H), 7.96 (d, J = 1.9 Hz, 1H), 7.90–7.85 (m, 2H), 7.79 (dd, J = 8.4, 2.0 Hz, 1H), 7.76–7.72 (m, 1H), 7.53 (s, 1H), 7.44–7.36 (m, 3H), 6.64 (q, J = 2.7, 2.2 Hz, 1H), 5.88 (dq, J = 3.7, 2.4, 1.9 Hz, 2H), 5.75 (dd, J = 11.9, 5.8 Hz, 1H), 3.75 (s, 3H). ^{13}C NMR (126 MHz, DMSO) δ 165.76, 164.37, 163.76, 159.80, 151.86, 145.32, 143.92, 135.44, 132.54, 131.72, 131.46, 131.25, 130.92, 128.22, 128.02, 127.95, 126.05, 122.71, 116.31, 114.53, 106.64, 106.32, 56.91, 56.67,41.84, 34.20, 34.18. HPLC-UV (254 nm) for $C_{24}H_{19}Cl_2FN_6O_3S_2$ ESI-MS, purity: 95.2%. LC-MS (*m*/*z*): 591.42 $[M - H]^-$.

***N*′-(2-(3-(3,4-Dichlorophenyl)-5-(1-methyl-1*H*-pyrrol-2-yl)-4,5-dihydro-1*H*-pyrazol-1-yl)thiazole-4-carbonyl)butane-1-sulfonohydrazide (10c).** To a solution of **8** (100 mg, 0.23 mmol) in DMF (10 mL) and cooled to 0 °C, butane-1-sulfonyl chloride (37 mg, 0.23 mmol) was added dropwise and then the reaction mixture was stirred at room temperature for 10 h. When the reaction is finished, distilled water (25 mL) was added and the formed precipitate that formed was filtered, washed with water and dried under high vacuum. The formed precipitate was recrystallized from ethanol yielding **10c** (80 mg, 65%) of as yellow solid. ^{1}H NMR (500 MHz, DMSO-d_6) δ 9.75 (d, J = 2.7 Hz, 1H), 9.52 (d, J = 2.7 Hz, 1H), 7.97 (d, J = 2.0 Hz, 1H), 7.82–7.73 (m, 2H), 7.68 (s, 1H), 6.64 (t, J = 2.3 Hz, 1H), 5.92–5.85 (m, 2H), 5.80 (dd, J = 11.8, 5.7 Hz, 1H), 3.95 (dd, J = 17.9, 11.9 Hz, 1H), 3.78 (s, 2H), 3.50 (dd, J = 17.9, 5.7 Hz, 1H), 3.10–3.02 (m, 2H), 1.81–1.71 (m, 2H), 1.39 (q, J = 7.4 Hz, 2H), 0.90 (t, J = 7.4 Hz, 3H). ^{13}C NMR (126 MHz, DMSO-d_6) δ 164.46, 160.51, 151.91, 144.11, 132.55, 131.95, 131.72, 131.39, 131.26, 128.24, 126.50, 122.83, 116.46, 106.87, 106.68, 57.03, 51.79, 41.84, 34.20, 25.12, 21.08, 13.62. HPLC-UV (254 nm) for $C_{22}H_{24}Cl_2N_6O_3S_2$ ESI-MS, purity: 97.1%. LC-MS (*m*/*z*): 553.43 $[M - H]^-$.

2-(3-(3,4-Dichlorophenyl)-5-(1-methyl-1*H*-pyrrol-2-yl)-4,5-dihydro-1*H*-pyrazol-1-yl)thiazol-4(5*H*)-one (11). To a solution of pyrazol-1-ylthiocarboxamide **5** (0.05 g, 0.141 mmol), in ethanol (2 mL), ethyl bromoacetate (0.024 g, 0.14 mmol) was added dropwise. The resulting mixture was heated under reflux for 3 h, and the solvent was subsequently evaporated under reduced pressure. The remaining substance was purified by recrystallization from ethanol and drying, producing **11** as a white solid with a yield of (0.037 g, 83%). ^{1}H NMR (600 MHz, DMSO-d_6) δ 8.02 (d, J = 2.0 Hz, 1H), 7.84 (dd, J = 8.4, 2.0 Hz, 1H), 7.79 (d, J = 8.4 Hz, 1H), 6.67 (t, J = 2.2 Hz, 1H), 5.92–5.81 (m, 3H), 4.01 (dd, J = 18.2, 11.3 Hz, 1H), 3.93 (d, J = 1.3 Hz, 2H), 3.58 (dd, J = 18.3, 4.4 Hz, 1H). ^{13}C NMR (151 MHz, DMSO-d_6) δ 186.99, 177.79, 158.68, 134.02, 132.10, 131.42, 130.78, 130.71, 129.15, 127.21, 122.96, 106.92, 106.23, 56.98, 42.38, 38.93, 34.10. HPLC-UV (254 nm) for $C_{17}H_{14}Cl_2N_4OS$ ESI-MS, purity: 96%. LC-MS (*m*/*z*): 393.11 $[M - H]^-$.

General procedure for the synthesis of compounds 12a–c

To a flask containing compound **11** (0.02 g, 0.051 mmol) dissolved in 1 mL ethanol, a suitable aldehyde (0.007 g, 0.051 mmol), and piperidine (0.05 mL) were added and the reaction mixture was heated under reflux at 100 °C for 4 h. After cooling, the resulting powder was filtered, washed with methanol, and recrystallized with ethanol yielding compounds **12a–c**.

(*E*)-2-(3-(3,4-Dichlorophenyl)-5-(1-methyl-1*H*-pyrrol-2-yl)-4,5-dihydro-1*H*-pyrazol-1-yl)-5-(4-fluorobenzylidene)thiazol-4(5*H*)-one (12a). Compound **11** (0.02 g, 0.051 mmol), 4-fluorobenzaldehyde (0.007 g, 0.051 mmol), and piperidine (0.05 mL) were heated under reflux for 4 h in ethanol (1 mL). After cooling, the resulting powder was filtered, washed with methanol, and recrystallized with ethanol yielding **12a** (0.018 g, 73%) as a buff solid. ^{1}H NMR (600 MHz, DMSO-d_6) δ 8.02 (d, J = 2.0 Hz, 1H), 7.84 (dd, J = 8.4, 2.0 Hz, 1H), 7.79 (d, J = 8.4 Hz, 1H), 6.67 (t, J = 2.2 Hz, 1H), 5.91–5.81 (m, 3H), 4.01 (dd, J = 18.3, 11.4 Hz, 1H), 3.93 (d, J = 1.3 Hz, 2H), 3.74 (s, 3H), 3.57 (dd, J = 18.2, 4.5 Hz, 1H). HPLC-UV (254 nm) for $C_{24}H_{17}Cl_2FN_4OS$ ESI-MS, purity: 95.6%. LC-MS (m/z): 499.22 $[M + H]^+$.

(*E*)-2-(3-(3,4-Dichlorophenyl)-5-(1-methyl-1*H*-pyrrol-2-yl)-4,5-dihydro-1*H*-pyrazol-1-yl)-5-(3-fluorobenzylidene)thiazol-4(5*H*)-one (12b). Compound **11** (0.03 g, 0.076 mmol), 3-fluorobenzaldehyde (0.01 g, 0.076 mmol), and piperidine (0.08 mL) were heated under reflux for 4 h in ethanol (2 mL). After cooling, the resulting powder was filtered, washed with methanol, and recrystallized with ethanol yielding **12b** (0.031 g, 81%) as a white solid. ^{1}H NMR (600 MHz, DMSO-d_6) δ 8.03 (d, J = 2.0 Hz, 1H), 7.85 (dd, J = 8.4, 2.0 Hz, 1H), 7.80 (d, J = 8.4 Hz, 1H), 6.68 (dd, J = 2.6, 1.8 Hz, 1H), 5.93–5.82 (m, 3H), 4.02 (dd, J = 18.3, 11.3 Hz, 1H), 3.94 (d, J = 1.3 Hz, 2H), 3.75 (s, 3H), 3.58 (dd, J = 18.3, 4.4 Hz, 1H). ^{13}C NMR (151 MHz, DMSO-d_6) δ 187.00, 177.80, 158.68, 134.03, 132.11, 131.43, 130.79, 130.72, 129.15, 127.21, 122.98, 106.93, 106.24, 56.99, 42.40, 38.94, 34.11. HPLC-UV (254 nm) for $C_{24}H_{17}Cl_2FN_4OS$ ESI-MS, purity: 96.4%. LC-MS (m/z): 499.25 $[M + H]^+$.

(*E*)-5-(3-Chloro-4-fluorobenzylidene)-2-(3-(3,4-dichlorophenyl)-5-(1-methyl-1*H*-pyrrol-2-yl)-4,5-dihydro-1*H*-pyrazol-1-yl)thiazol-4(5*H*)-one (12c). Compound **11** (0.03 g, 0.076 mmol), 3-chloro-4-fluorobenzaldehyde (0.012 g, 0.076 mmol), and piperidine (0.08 mL) were heated under reflux for 4 h in ethanol (2 mL). After cooling, the resulting powder was filtered, washed with methanol, and recrystallized with ethanol yielding **12c** (0.028 g, 71%) as a yellow solid. ^{1}H NMR (600 MHz, DMSO-d_6) δ 8.04 (d, J = 2.0 Hz, 1H), 7.85 (dd, J = 8.4, 2.0 Hz, 1H), 7.81 (d, J = 8.4 Hz, 1H), 6.68 (t, J = 2.2 Hz, 1H), 5.91–5.83 (m, 3H), 4.02 (dd, J = 18.4, 11.3 Hz, 1H), 3.95 (d, J = 1.2 Hz, 2H), 3.75 (s, 3H), 3.59 (dd, J = 18.3, 4.5 Hz, 1H). ^{13}C NMR (151 MHz, DMSO-d_6) δ 186.99, 177.80, 158.68, 134.03, 132.11, 131.43, 130.79, 130.72, 129.15, 127.21, 122.97, 106.93, 106.24, 56.99, 42.39, 38.94, 34.11. HPLC-UV (254 nm) for $C_{24}H_{16}Cl_3FN_4OS$ ESI-MS, purity: 96.4%. LC-MS (m/z): 533.12 $[M + H]^+$.

Gene expression analysis

RNA isolation and reverse transcription (RT) reaction. Total RNA was isolated from MCF-7, A549, and PC3 cell lines using the RNeasy Mini Kit (Qiagen, Hilden, Germany) with an additional DNaseI (Qiagen) digestion step, following the manufacturer's protocol. The isolated RNA was treated with RQ1 RNase-free DNase (Invitrogen, Germany) to remove DNA residues, re-suspended in DEPC-treated water, and quantified spectrophotometrically at 260 nm. RNA purity was confirmed with a 260/280 nm ratio of 1.8 to 2.1.[18,19] RNA integrity was further verified using ethidium bromide-stained agarose gel electrophoresis to visualize the 28S and 18S rRNA bands. Aliquots of RNA were either used immediately for reverse transcription (RT) or stored at −80 °C for later use.[20,21]

For cDNA synthesis, 5 μg of total RNA from MCF-7, A549, and PC3 cell lines was reverse transcribed using the RevertAid™ First Strand cDNA Synthesis Kit (Fermentas, Germany) in a 20 μL reaction volume. The master mix included 50 mM MgCl2, 10× RT buffer (50 mM KCl; 10 mM Tris–HCl; pH 8.3), 10 mM of each dNTP, 50 μM oligo-dT primer, 20 IU ribonuclease inhibitor, and 50 IU MuLV reverse transcriptase. Each sample mixture was centrifuged for 30 seconds at 1000 g before transferring to a thermocycler. The RT reaction proceeded at 25 °C for 10 minutes, 42 °C for 1 hour, and concluded with a denaturation step at 99 °C for 5 minutes. The reaction tubes were then flash-cooled on ice and stored until use for cDNA amplification *via* quantitative Real Time PCR (qRT-PCR).

Quantitative real time-PCR (qRT-PCR). The cDNA copy number for MCF-7, A549, and PC3 cell lines was determined using the StepOne™ Real-Time PCR System from Applied Biosystems (Thermo Fisher Scientific, Waltham, MA, USA). PCR reactions were prepared in 25 μL volumes containing 12.5 μL of 1× SYBR® Premix Ex Taq™ (TaKaRa, Biotech. Co. Ltd.), 0.5 μL of 0.2 μM sense primer, 0.5 μL of 0.2 μM antisense primer, 6.5 μL of distilled water, and 5 μL of cDNA template. The PCR protocol consisted of three stages: an initial step at 95.0 °C for 3 minutes, followed by 40 cycles with three steps each (95.0 °C for 15 seconds, 55.0 °C for 30 seconds, and 72.0 °C for 30 seconds), and a final stage of 71 cycles starting at 60.0 °C, increasing by 0.5 °C every 10 seconds up to 95.0 °C. Each experiment included a distilled water control. Specific primers for the cancer-related genes Bcl-2, BAX, p53, and Caspase-3[17,18] for MCF-7, A549, and PC3 cell lines were designed and listed in Table 1. At the end of each qPCR, a melting curve analysis at 95.0 °C was performed to verify primer quality. Relative quantification of target genes to the reference was determined using the $2^{-\Delta\Delta C_T}$ method.[22,23]

DNA damage using the comet assay. DNA damage in MCF-7, A549, and PC3 cancer cell lines was assessed using the comet assay following Olive *et al.* (1990).[24] After trypsin treatment to create a single-cell suspension, approximately 1.5 × 10^4 cells were embedded in 0.75% low-gelling-temperature agarose and quickly pipetted onto pre-coated microscope slides. Samples were lysed for 4 hours at 50 °C in 0.5% SDS, 30 mM EDTA, pH 8.0. They were then rinsed overnight at room temperature in Tris/borate/EDTA buffer, pH 8.0, followed by electrophoresis for 25 minutes at 0.6 V cm^{-1} and staining with propidium iodide. Slides were examined with a fluorescence microscope equipped with a CCD camera, and 150 individual comet images per sample were analyzed for tail moment, DNA content, and percentage of DNA in the tail. Approximately 100 cells per sample were examined to determine the percentage of cells with

DNA damage appearing as comets. Non-overlapping cells were randomly selected and visually scored on a scale of 0–3 based on comet tail length and relative DNA content in the nucleus: class 0 = no detectable DNA damage; class 1 = tail length less than the nucleus diameter; class 2 = tail length between 1× and 2× the nuclear diameter; and class 3 = tail longer than 2× the nuclear diameter.[25]

Molecular docking. We conducted a molecular docking study to evaluate the potential anti-cancer effects of our newly developed 1,3,5-trisubstituted-1*H*-pyrazole derivatives (**6c**, **8**, **10b**, and **10c**) by targeting the Bcl-2 protein. This analysis included examining the binding modes and affinities of these compounds within the Bcl-2 protein's active sites. To begin, we obtained the X-ray crystal structures of the Bcl-2 protein from the Protein Data Bank (**https://www.rcsb.org**) using the PDB code 4AQ3.[26] The receptor preparation for docking was carried out using Biovia Discovery Studio,[27] which involved removing unnecessary chains and water molecules, adding polar hydrogens, and adjusting partial charges to create accurate receptor models suitable for docking simulations.

For the docking studies, we utilized the Autodock 4.2 software package. The process began with preparing coordinate files for both the ligands and the target protein, followed by the calculation of an affinity grid for the target. The grid box was set at dimensions of 50 × 50 × 50 with a grid point spacing of 0.375 Å, centered on the position of the co-crystallized ligand. The Lamarckian Genetic Algorithm (LGA) was employed to explore possible conformations, running ten iterations with up to 27 000 generations per iteration. The mutation rate was set at 0.02, and the crossover rate was 0.8. Multiple docking runs were performed using AutoDock 4.2 (ref. 28) to generate a variety of docked conformations. The best docking results were determined by evaluating the predicted binding energies and the consistency of the docking poses.

Ethical statement

This experimental study was carried out according to recommendations and under the regulations of the Medical Research Ethics Committee (MREC) at the National Research Centre in Egypt.

Data availability

The data supporting this article have been included as part of the ESI.†

Conflicts of interest

The authors declare no financial or commercial conflicts of interest.

Acknowledgements

The authors would like to thank National Research Centre, Cairo, Egypt and Menoufia University, Menoufia, Egypt for the financial support of this study.

References

1 M. S. Litwin and H.-J. Tan, The diagnosis and treatment of prostate cancer: A review, *JAMA, J. Am. Med. Assoc.*, 2017, **317**, 2532–2542.
2 R. J. Rebello, C. Oing, K. E. Knudsen, S. Loeb, D. C. Johnson, R. E. Reiter, S. Gillessen, T. Van der Kwast and R. G. Bristow, Prostate cancer, *Nat. Rev. Dis. Primers*, 2021, **7**, 1–27.
3 R. Elancheran, K. Saravanan, S. Divakar, S. Kumari, V. L. Maruthanila, S. Kabilan, M. Ramanathan, R. Devi and J. Kotoky, Design, synthesis and biological evaluation of novel 1,3-thiazolidine-2,4-diones as anti-prostate cancer agents. Anti-Cancer Agents, *Med. Chem.*, 2017, **17**, 1756–1768.
4 S. Elmore, Apoptosis: A review of programmed cell death, *Toxicol. Pathol.*, 2007, **35**, 495–516.
5 B. Levine and G. Kroemer, Autophagy in the pathogenesis of disease, *Cell*, 2008, **132**, 27–42.
6 J. C. Reed, Bcl-2-family proteins and hematologic malignancies: History and future prospects, *Blood*, 2008, **111**, 3322–3330.
7 K. J. Campbell and S. W. G. Tait, Targeting BCL-2 regulated apoptosis in cancer, *Open Biol.*, 2018, **8**, 180002.
8 S. Pattingre, A. Tassa, X. Qu, R. Garuti, X. H. Liang, N. Mizushima, M. Packer, M. D. Schneider and B. Levine, Bcl-2 antiapoptotic proteins inhibit Beclin 1-dependent autophagy, *Cell*, 2005, **122**, 927–939.
9 M. Vogler, D. Dinsdale, M. J. Dyer and G. M. Cohen, Bcl-2 inhibitors: Small molecules with a big impact on cancer therapy, *Cell Death Differ.*, 2009, **16**, 360–367.
10 R. T. Marquez and L. Xu, Bcl-2:Beclin 1 complex: Multiple mechanisms regulating autophagy/apoptosis toggle switch, *Am. J. Cancer Res.*, 2012, **2**, 214–221.
11 X. Dong, Q. Liang, Y. Z. Pan, X. Wang, Y. C. Kuo, W. C. Chiang, X. Zhang, N. S. Williams, J. Rizo, B. Levine and J. K. De Brabander, Novel Bcl-2 inhibitors selectively disrupt the autophagy-specific Bcl-2-Beclin 1 protein-protein interaction, *ACS Med. Chem. Lett.*, 2022, **13**, 1510–1516.
12 K.-M. Qiu, H.-H. Wang, L.-M. Wang, Y. Luo, X.-H. Yang, X.-M. Wang and H.-L. Zhu, Design, Synthesis and Biological Evaluation of Pyrazolyl-Thiazolinone Derivatives as Potential EGFR and Her-2 Kinase Inhibitors, *Bioorg. Med. Chem.*, 2012, **20**(6), 2010–2018.
13 D. Havrylyuk, B. Zimenkovsky, O. Vasylenko, L. Zaprutko, A. Gzella and R. Lesyk, Synthesis of Novel Thiazolone-Based Compounds Containing Pyrazoline Moiety and Evaluation of Their Anticancer Activity, *Eur. J. Med. Chem.*, 2009, **44**(4), 1396–1404.
14 D. Havrylyuk, B. Zimenkovsky, O. Vasylenko, A. Gzella and R. Lesyk, Synthesis of New 4-Thiazolidinone-, Pyrazoline-, and Isatin-Based Conjugates with Promising Antitumor Activity, *J. Med. Chem.*, 2012, **55**(20), 8630–8641.
15 N. M. Boshta, A. Temirak, Z. A. El-Shahid, Z. Shafiq and A. A. F. Soliman, Design, synthesis, molecular docking and biological evaluation of 1,3,5-trisubstituted-1H-pyrazole

derivatives as anticancer agents with cell cycle arrest, ERK and RIPK3-kinase activities, *Bioorg. Chem.*, 2024, **143**, 107058.

16 G. Rajendran, D. Bhanu, B. Aruchamy, P. Ramani, N. Pandurangan, K. N. Bobba, E. J. Oh, H. Y. Chung, P. Gangadaran and B.-C. Ahn, Chalcone: A Promising Bioactive Scaffold in Medicinal Chemistry, *Pharmaceuticals*, 2022, **15**, 1250.

17 F. A. Carey and R. J. Sundberg, *Advanced Organic Chemistry Part A: Structure and Mechanisms*, Springer Science, New York, 5th edn, 2007.

18 S. A. A. Linjawi, E. A. Sharafeldin, W. K. B. Khalil and H. F. Booles, Potential role of Jasonia montana and Jasonia candicans against Alzheimer's disease: assessment of oxidative stress and gene expression changes in AD-induced rats, *Egypt. J. Genet. Cytol.*, 2011, **40**, 61–80.

19 S. Y. Elateek, L. M. Salem, E. S. Ahmed and W. K. B. Khalil, Staphylococcus aureus isolates from hospital clinics induce ROS-mediated DNA damage, apoptosis, and gene expression alterations in male mice, *Gene Rep.*, 2021, **23**, 101028.

20 A. F. Brito, A. M. Abrantes, C. Pinto-Costa, A. R. Gomes, A. C. Mamede, J. Casalta-Lopes, A. C. Gonçalves, A. B. Sarmento-Ribeiro, J. G. Tralhão and M. F. Botelho, Hepatocellular carcinoma and chemotherapy: The role of p53, *Chemotherapy*, 2012, **58**, 381–386.

21 M. A. Ramadan, A. E. Shawkey, M. A. Rabeh and A. O. Abdellatif, Expression of P53, BAX, and BCL-2 in human malignant melanoma and squamous cell carcinoma cells after tea tree oil treatment *in vitro*, *Cytotechnology*, 2019, **71**, 461–473.

22 M. A. Elhinnawi, R. M. Mohareb, H. M. Rady, W. K. B. Khalil, M. M. Abd Elhalim and G. A. Elmegeed, Novel pregnenolone derivatives modulate apoptosis *via* Bcl-2 family genes in hepatocellular carcinoma *in vitro*, *J. Steroid Biochem. Mol. Biol.*, 2018, **183**, 125–136.

23 W. K. B. Khalil, W. Zarouk, G. Nour Eldeen, A. Ramadan, A. Fayez, N. Esmaiel, B. Foda, K. Hamed, S. M. Kassem and H. El-Bassyouni, Apoptosis, reactive oxygen species and DNA damage in familial Mediterranean fever patients, *Gene Rep.*, 2019, **14**, 76–80.

24 P. L. Olive, J. P. Banáth and R. E. Durand, Heterogeneity in radiation-induced DNA damage and repair in tumor and normal cells measured using the "comet" assay, *Radiat. Res.*, 2012, **178**, AV35–AV42.

25 A. Collins, M. Dusinska, M. Franklin, M. Somorovska, H. Petrovska, S. Duthie, L. Fillion, M. Panayiotidis, K. Raslova and N. Vaughan, Comet assay in human biomonitoring studies: Reliability, validation, and applications, *Environ. Mol. Mutagen.*, 1997, **30**, 139–146.

26 H. L. Perez, P. Banfi, J. Bertrand, Z. W. Cai, J. W. Grebinski, K. Kim, J. Lippy, M. Modugno, J. Naglich, R. J. Schmidt, A. Tebben, P. Vianello, D. D. Wei, L. Zhang, A. Galvani, L. J. Lombardo and R. M. Borzilleri, Identification of a phenylacylsulfonamide series of dual Bcl-2/Bcl-xL antagonists, *Bioorg. Med. Chem. Lett.*, 2012, **22**, 3946–3950.

27 BIOVIA and Dassault Systèmes, *BIOVIA Discovery Studio Visualizer, 2021*, Dassault Systèmes, San Diego, 2023, **https://www.3ds.com/**.

28 G. M. Morris, R. Huey, W. Lindstrom, M. F. Sanner, R. K. Belew, D. S. Goodsell and A. J. Olson, AutoDock4 and AutoDockTools4: Automated docking with selective receptor flexibility, *J. Comput. Chem.*, 2009, **30**, 2785–2791.